JACS
JOURNAL OF THE AMERICAN CHEMICAL SOCIETY

Article

pubs.acs.org/JACS

Developing a Gel-Based Sensor Using Crystal Morphology Prediction

Gesine K. Veits, Kelsey K. Carter, Sarah J. Cox, and Anne J. McNeil*

Department of Chemistry and Macromolecular Science and Engineering Program, University of Michigan, 930 North University Avenue, Ann Arbor, Michigan 48109-1055, United States

Supporting Information

ABSTRACT: The stimuli-responsive nature of molecular gels makes them appealing platforms for sensing. The biggest challenge is in identifying an appropriate gelator for each specific chemical or biological target. Due to the similarities between crystallization and gel formation, we hypothesized that the tools used to predict crystal morphologies could be useful for identifying gelators. Herein, we demonstrate that new gelators can be discovered by focusing on scaffolds with predicted high aspect ratio crystals. Using this morphology prediction method, we identified two promising molecular scaffolds containing lead atoms. Because solvent is largely ignored in morphology prediction but can play a major role in gelation, each scaffold needed to be structurally modified before six new Pb-containing gelators were discovered. One of these new gelators was developed into a robust sensor capable of detecting lead at the U.S. Environmental Protection Agency limit for paint (5000 ppm).

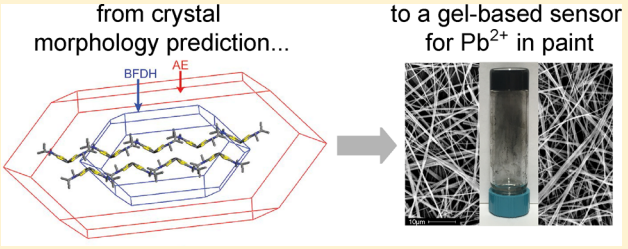

INTRODUCTION

With applications ranging from sensing[1] to biomedicine[2] to environmental remediation,[3] molecular gels have caught the attention of researchers across diverse fields.[4] Most gelators are discovered serendipitously because a priori prediction tools are largely nonexistent.[5] As a result, the most challenging step in developing a new gel-based application is identifying an appropriate gelator. Recently, Adams and Berry used a computational model to identify new dipeptide-based gelators based on experimental quantitative structure−property relationships.[6] Herein we describe an alternative computational model based on crystal morphology prediction. To test the utility of this model in driving new applications, we targeted a gel-based sensor for lead paint.

Lead-containing paint was banned in the United States in 1978.[7] Despite this ban, many buildings, including homes, schools, and businesses, still contain deteriorating remnants of the paint. One major risk associated with toxic lead paint is ingestion of particles by children, as even low levels of lead poisoning can impair cognitive development.[8] Of course, adults are also at risk, especially from dust generation during home renovations or when stripping old paint without proper safety measures.[9] Three major drawbacks associated with current at-home lead-detection kits are false negative results,[10] their reliance on colorimetric changes, and detecting lead at concentrations lower than mandated by the U.S. Environmental Protection Agency (EPA), which can substantially increase the cost of renovations. Other methods, such as professional X-ray fluorescence analysis or ex situ lab testing are prohibitive due to their cost. The solution-to-gel transition is both unambiguous and independent of paint color; as such, we set out to develop a molecular gel-based sensor for lead paint. Our approach to new gelator discovery is rooted in the similarities between crystallization and gel formation.

Solid-state assembly into crystalline, semicrystalline, and amorphous forms is important to many fields, including pharmaceuticals, explosives, heterogeneous catalysis, and molecular gels. Bulk properties such as dissolution rate, density, porosity, and modulus are strongly influenced by the solid-state structure. As a result, many research efforts have focused on methods for predicting solid-state forms.[11] The largest advances have been in the field of crystallization, where one can predict the crystal morphology from a known crystal structure.[12]

Crystal morphology prediction dates back to the late 19th century when Bravais, Friedel, Donnay, and Harker (BFDH)[13] proposed a method that focuses on lattice spacing (distance between crystal planes) to predict crystal morphology. Later, Hartman and Perdok expanded on the BFDH model to directly consider the role of intermolecular interactions in crystal morphology.[14] They postulated that stronger intermolecular interactions (or larger attachment energies (AE)[15]) between the crystal planes leads to faster growth rates. Using the AE method, the predicted crystal morphologies offer a visual representation of the intermolecular interactions in each dimension. Overall, the Hartman−Perdok approach has provided accurate morphologies in many different cases and, as a result, is widely implemented.[16] We hypothesized that these morphology prediction methods could be used to discover new molecular gelators because the self-assembly processes in crystallization may be similar to gel formation.[17]

The links between crystallization and gel formation have been the focus of research efforts for some time.[18] Hanabusa

Received: June 23, 2016
Published: September 6, 2016

DOI: 10.1021/jacs.6b06269
J. Am. Chem. Soc. 2016, 138, 12228−12233

and co-workers postulated that one-dimensional (1D) intermolecular interactions are needed to form the anisotropic fibers commonly observed in gels.[19] Toward this goal, we and others have used the Cambridge Structural Database (CSD)[20] as a source of inspiration for new gelators.[21] As an example, Dastidar identified nine new gelators from a group of 32 ammonium salts that exhibited a 1D hydrogen-bonding network in the crystal structure.[21a] We identified a new gelator by searching the CSD for 1D Hg−arene interactions.[21b] Although this approach has been successful, the selection process is both subjective and time-consuming. Moreover, less obvious intermolecular interactions (e.g., van der Waals) and the effect of solvent, which can be important in gel formation,[22] are overlooked in this approach. Based on our previous results, wherein gelators exhibited stronger intermolecular interactions than nongelators,[23] we modified our design strategy to focus not just on the directionality of the interactions but also their relative strength. It is here where the parallels between crystallization and gelation provided the inspiration to pursue morphology prediction methods as a means to new application-guided gelator discovery.

We report herein a new sensor for lead in paint developed by successfully using morphology prediction tools to identify new molecular scaffolds starting from known crystal structures. We anticipate that this method will greatly expand the utility of low molecular weight gels as soft materials by enabling rapid gelator discovery for specific applications.

RESULTS AND DISCUSSION

We began our investigations by searching the CSD for lead-containing crystal structures. The CSD contains over 800 000 crystal structures. Therefore, to obtain a tractable data set several search criteria were used to narrow the data set. For example, we only considered lead-containing crystal structures that were ordered, were error-free, and did not contain free ions or solvents. Overall, this filtering process led to a total of 352 Pb(II) and Pb(IV) complexes. Each structure was then optimized within Materials Studio.[24] This step is necessary because crystallography tends to systematically underestimate bond lengths involving hydrogens.[25]

The Universal Force Field (UFF) was selected for this geometry optimization because it can accommodate Pb.[26] Because the UFF requires a tetrahedral geometry for Pb, all Pb(IV) compounds and all Pb(II) sandwich compounds were removed from the data set at this point,[27] reducing the number of unique compounds investigated to 184. The geometry optimization can be performed by either holding the unit cell parameters constant or not. We found that these constrained geometry calculations led to smaller changes between the optimized and experimental structures (Figure S15 and Tables S2 and S3).[28] As a consequence, the geometry optimization is less likely to change the interactions present in the experimental structure.[24,29]

After the geometry optimization was completed, a crystal graph, which provides insight into the relative importance of each intermolecular interaction, was generated in Materials Studio (Scheme 1). The crystal graph describes the interaction energy between the center of mass of one molecule with all other molecules in a given sphere. The sphere can be defined by one or more unit cells. We found that a similar morphology was predicted (i.e., the aspect ratios were within 15% of each other) regardless of the interaction sphere size (Tables S4 and S5). We therefore selected a radius of one unit cell to place an emphasis on the shorter range, directional intermolecular interactions that likely drive gel formation.

Scheme 1. Visualizing the Intermolecular Interactions

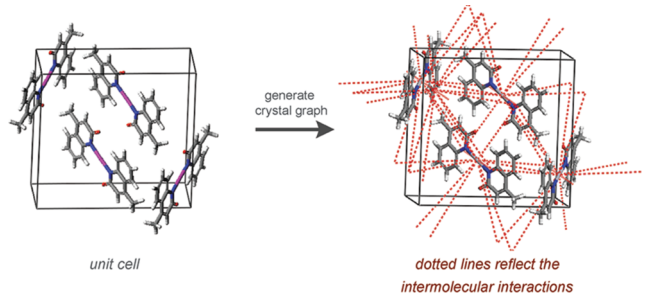

From the crystal graph we predicted the crystal morphology using the Growth Morphology software within Materials Studio,[24] which is based on the Hartman−Perdok analysis of AEs.[15,30] For comparison, the morphologies were also calculated using the BFDH method. Since this approach relies on distances, no force field is needed. Aspect ratios, which were obtained by dividing the longest distance within a crystal by the shortest distance (Scheme S1), for all 184 compounds can be found in Table S8 and Figure S17.

A few general trends were observed. For example, when the aspect ratios were equal to or less than 2, both the BFDH and AE methods predicted similar values (Figure S17). In contrast, as the AE aspect ratios increased ($AR_{AE} > 2$), the BFDH aspect ratios remained low (Figure 1A). It is important to note that both theories generally predicted the same crystal faces, but in different proportions (Figure 1B,C). Therefore, these differences at high AE aspect ratio suggest that the BFDH method underemphasizes interactions that are prominent in one or two dimensions.

To narrow the list to a reasonable number of synthetic targets, the compounds with the highest (top 5%) aspect ratios were selected for further evaluation (Table S9). The predicted morphologies of all nine compounds can be found in Figures S18−S26. With a user-friendly at-home chemical sensor for lead paint as our target application, we focused on compounds that were both air- and moisture-tolerant. In addition, we only selected compounds that could be synthesized in one pot from commercially available reagents and involved no more than one ligand class per complex. Based on these criteria, compounds **1a** (CSD entry: NAYNUW01)[31] and **2a** (CSD entry: NUNXOK)[32] were chosen for synthesis, derivatization, and gel screening.

As shown in Figure 1B,C, compound **1a** exhibits 1D Pb−S intermolecular interactions, which align with the long axis of the needle-shaped crystal. We anticipated that either **1a** or a related derivative might form gel fibers via the same Pb−S-promoted self-assembly mechanism. Compound **2a** displays π-stacking, as well as an analogous 1D Pb−O intermolecular interaction, that aligns with the needle's long-axis. Again, we anticipated that either **2a** or a related derivative might form a gel via similar intermolecular interactions. To test this hypothesis, we synthesized compounds **1a**−**h** and **2a**,**b** in high yields via one-pot reactions and evaluated their gelation ability (Chart 1).

The as-synthesized derivatives were screened for gel formation in a variety of polar/nonpolar and organic/aqueous solvents. At the time we started this work, there were no known gelators that incorporate Pb(II).[33] Although neither **1a**−**c** nor

DOI: 10.1021/jacs.6b06269
J. Am. Chem. Soc. 2016, 138, 12228−12233

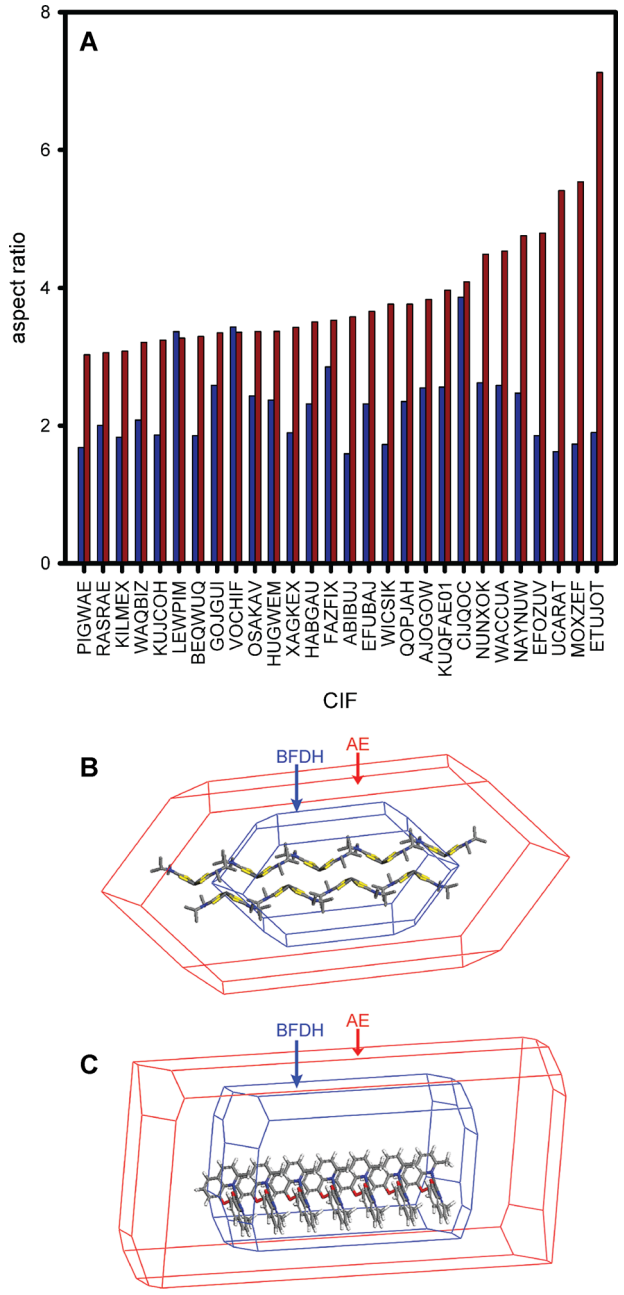

Figure 1. (A) Plot of the highest aspect ratios predicted by the BFDH (blue) and AE (red) methods. Predicted morphologies for compounds **1a** (B) and **2a** (C).

2a formed gels under any of the conditions tested, **1d**–**h** and **2b** did form gels (Tables S11–S13). Moreover, **1d**–**h** formed stable gels in solvents relevant to sensing lead paint, including paint thinner, acetone and methyl ethyl ketone (MEK) (Tables S11 and S13). Rheological studies of each gel revealed that the storage modulus (G') was at least 1 order of magnitude higher than the loss modulus (G''), which is characteristic of small-molecule gels (Figures S29–S35).[34] Moreover, scanning electron microscopy revealed that the morphologies consisted of high aspect ratio fibers (~0.1–3 μm in diameter), which is also characteristic of molecular gels (Figure 2 and Figures S36–S42).

To determine whether the Pb–S and Pb–O intermolecular interactions observed in the crystal structures were involved in

Chart 1

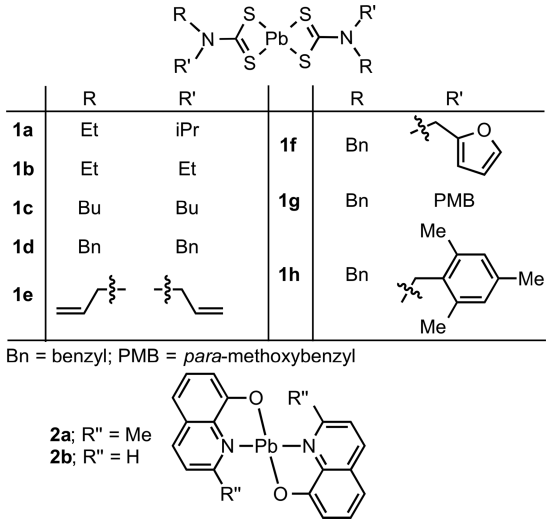

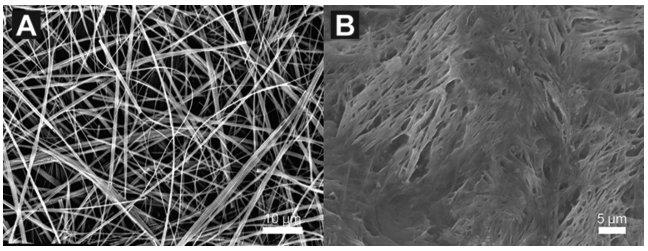

Figure 2. Scanning electron microscopy images of (A) **1d** (2.7 mM in acetone) and (B) **2b** (13.9 mM in H_2O/EtOH with pH = 12).

gelation, we attempted to grow single crystals of each gelator to compare their diffraction patterns to the corresponding gels. Unfortunately, we were unable to grow single crystals suitable for X-ray analysis for **1d**–**h** and **2b** in gelling solvents. However, a crystal structure of **2b** was known (CSD entry: FOHFEO).[35] Interestingly, it was predicted to have a low aspect ratio. Nevertheless, the (simulated) diffraction pattern for the crystal was different than the observed diffraction pattern for the wet (and dry) gel (Figure S44).[36,37] As a consequence, the molecular packing in this crystal is likely unrelated to that in the gel.

Overall, these results highlight one limitation of this approach: self-assembly depends on both the molecular structure and solvent structure. The reported crystal structures—our starting point—consider just one molecular and solvent structure (i.e., the crystallization conditions). As a consequence, what we identify using the morphology prediction approach is a series of scaffolds that form 1D assemblies under the crystallization conditions. These 1D assemblies might (or might not) translate to another set of closely related conditions (structure/solvent). Empirically, the approach works: six new gelators were discovered with minor scaffold derivatization and solvent screening. Nevertheless, at this time, we are unable to determine whether the apparent driving forces for the 1D assemblies observed in the crystal structures bear any resemblance to the molecular packing within the gel.

With several gelators in hand, we explored their ability to detect lead in paint. We focused on **1d** since the starting materials are commercially available and it forms stable gels in a

DOI: 10.1021/jacs.6b06269
J. Am. Chem. Soc. 2016, 138, 12228–12233

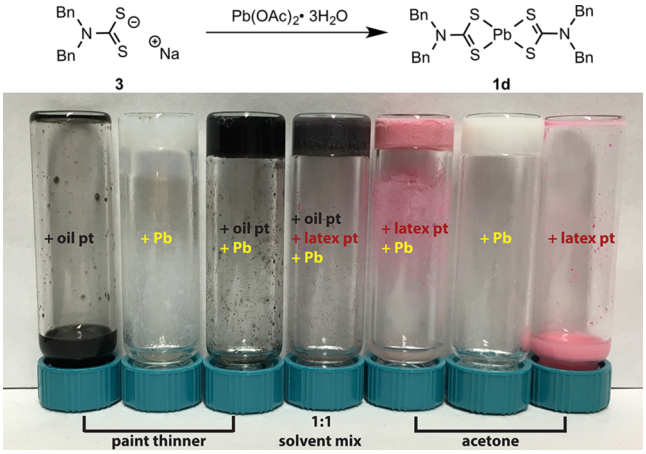

Figure 3. In situ Pb-triggered gelation with oil-based (black) and latex-based (pink) paint (pt) in paint thinner and acetone ([**3**] = 13−14 mM; [$Pb(OAc)_2$] = 6.3−7.6 mM; total vol = 1 mL).

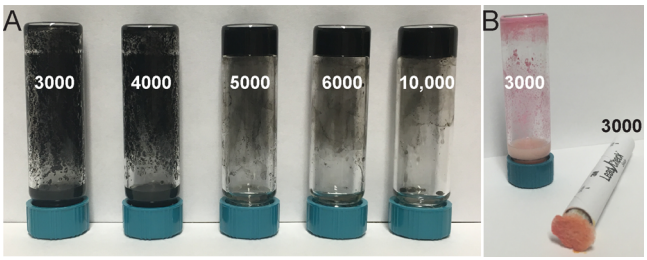

Figure 4. (A) Gelation observed at 10 000, 6000, and 5000 ppm with no gelation at 3000 and 4000 ppm Pb^{2+}. (B) Using a dry (pink) paint sample, the commercially available lead test gives a positive signal (pink coloration) at 3000 ppm while no gel forms at that Pb^{2+} concentration. A control showed no coloration of the swab when Pb was absent (Figure S50).

wide range of relevant solvents. A sodium dibenzylcarbamodithioate salt (**3**) was prepared to test in situ formation of lead complex **1d**, thereby triggering gelation (Figure 3). The lead salts most commonly found in paint include lead carbonate, lead chromate and lead oxide. Therefore, we evaluated several different lead salts in our studies. Gratifyingly, we observed immediate Pb-complex formation and gelation when using PbO, $PbCO_3$, $PbCrO_4$, and $Pb(OAc)_2{\cdot}3H_2O$ (Table S15 and Figure S46).[38] Only $Pb(NO_3)_2$ did not produce a stable gel, although fiber formation was observed. Having established that in situ gelation is feasible, we focused on sensing in the presence of paint.

The unambiguous solution-to-gel phase transition, identifiable by nonexperts and unaffected by sample color, is the crux of this new sensing platform. We began our studies with oil-based paint (and paint thinner[39]) because most lead-contaminated paint is oil-based.[40] Gels immediately formed in paint thinner in the presence of oil-based paint, while no gel formed in the absence of lead. As evident in Figure 3, the gel is easily identifiable regardless of the presence of paint or the paint color—a significant advantage over current at-home test kits.[10] For comparison, the analogous tests were run with acetone and pink latex-based paint. Remarkably, the gel still formed when paint thinner and acetone were mixed and both types of paint were added, demonstrating the versatility of this sensor.

Because a variety of metal salts can be present in paint, we examined the specificity of the sensor. Adding **3** to solutions containing acetate salts of Ni^{2+}, Ca^{2+}, Cd^{2+}, Ba^{2+}, Cu^{2+}, Zn^{2+}, Mn^{2+}, and Fe^{2+} did not result in gels (Table S16 and Figure S47). Most likely, the dithiocarbamate formed complexes with these metals[41] but the resulting products were not gelators either due to unfavorable geometries or intermolecular interactions. Importantly, Pb-triggered gelation was unaffected by high concentrations of these other metal salts when excess ligand was added (Table S17, Figure S48, Table S29, and Table S30).

Finally, we wanted to sense lead at 5000 ppm—the concentration set by the EPA for at-home testing kits for lead in paint.[42] Because lead-based paint was unavailable, we mixed fresh paint with lead for the described sensor as a model. The critical gelation concentration (cgc) for in situ gelation with $PbCO_3$ in a 5000 ppm sample of oil-based paint was determined in paint thinner/methanol.[43] To ensure a homogeneous distribution of Pb^{2+} in paint, the paint samples were first diluted with paint thinner. Using the diluted wet paint, we found that all 10 samples with 5000 ppm lead resulted in a positive signal—formation of a gel (Figure 4A). Sensing at 10 000 and 6000 ppm was also successful, although one false negative was recorded from 10 samples. At 4000 ppm, 3 of 6 samples resulted in gel formation. Although fiber formation occurred at 3000 ppm lead, none of the samples formed gels, even if the sample was left to stand for 1 h (Table S25). A "blind" sensing experiment was performed to remove experimenter bias. Gels were observed in all seven vials containing lead at and above 5000 ppm while no gel formed in any of the five vials containing lead concentrations below 5000 ppm. In comparison, 3M's LeadCheck gave a positive result—red coloration—at 3000 ppm (Figure 4B).[44] Since our gel-based sensor is reliant on concentration, the detection limit can be adjusted to detect different concentrations of lead as needed, taking into account the amount of paint sample used for lead detection.[42] Finally, considering that a real-world application would require sensing from dried paint samples, we extended our method to dry paint. Unsurprisingly, the solvent and cgc had to be adjusted for this system. Nonetheless, we were able to sense lead at 5000 ppm, while no gels formed at 3000 ppm (Table S28).

CONCLUSIONS

In summary, we demonstrated herein that new gelators for specific applications can be discovered by focusing on scaffolds with predicted high aspect ratio crystal morphologies. These results are consistent with the notion that the driving forces for forming high aspect ratio crystals and gel fibers may be similarly guided by these directional intermolecular interactions. The success rate—6 of 10 compounds synthesized are gelators—is remarkably high compared to other approaches, including derivatizing known scaffolds[1b,c,5c] and previous CSD-based approaches.[21] Excitingly, this approach resulted in a new solution-to-gel phase transition-based sensor for lead in paint. Overall, we expect this simple approach for identifying new gelators to be useful for developing new molecular gel-based applications.

ASSOCIATED CONTENT

Supporting Information

The Supporting Information is available free of charge on the ACS Publications website at DOI: 10.1021/jacs.6b06269.

DOI: 10.1021/jacs.6b06269
J. Am. Chem. Soc. 2016, 138, 12228−12233

Experimental procedures; NMR spectra; morphology prediction procedure and data; gel formation experiments; rheological and SEM characterization of gels; PXRD data; in situ gelation in the presence of paint; sensing experiments (including Scheme S1, Figures S1−S50, and Tables S1−S30) (PDF)

AUTHOR INFORMATION

Corresponding Author

*ajmcneil@umich.edu

Notes

The authors declare no competing financial interest.

ACKNOWLEDGMENTS

We thank Dr. Danielle M. Zurcher, Dr. Antek Wong-Foy, and Jialiu Ma for helpful discussions, assistance with figure preparation, and powder X-ray diffraction. We thank Amanda K. Leone and Dr. Chen Kong for assistance with the blind sensing experiments. We thank the University of Michigan (Associate Professor Support Fund), Office of Naval Research (N000141210604), and the Camille and Henry Dreyfus Foundation (Teacher-Scholar Award) for support of this work. K.K.C. thanks the NSF for a graduate research fellowship. S.J.C. thanks the University of Michigan for a position in its 2013 REU Site in the Chemical Sciences (NSF CHE-1062654).

REFERENCES

(1) (a) Ren, C.; Zhang, J.; Chen, M.; Yang, Z. *Chem. Soc. Rev.* **2014**, *43*, 7257. (b) Zurcher, D. M.; Adhia, Y. J.; Romero, J. D.; McNeil, A. J. *Chem. Commun.* **2014**, *50*, 7813. (c) Bremmer, S. C.; McNeil, A. J.; Soellner, M. B. *Chem. Commun.* **2014**, *50*, 1691. (d) Chen, J.; Wu, W.; McNeil, A. J. *Chem. Commun.* **2012**, *48*, 7310. (e) Bremmer, S. C.; Chen, J.; McNeil, A. J.; Soellner, M. B. *Chem. Commun.* **2012**, *48*, 5482. (f) Chen, J.; McNeil, A. J. *J. Am. Chem. Soc.* **2008**, *130*, 16496.

(2) (a) Skilling, K. J.; Citossi, F.; Bradshaw, T. D.; Ashford, M.; Kellam, B.; Marlow, M. *Soft Matter* **2014**, *10*, 237. (b) Tian, R.; Chen, J.; Niu, R. *Nanoscale* **2014**, *6*, 3474.

(3) (a) Okesola, B. O.; Smith, D. K. *Chem. Soc. Rev.* **2016**, *45*, 4226. (b) Carter, K. K.; Rycenga, H. B.; McNeil, A. J. *Langmuir* **2014**, *30*, 3522. (c) King, K. N.; McNeil, A. J. *Chem. Commun.* **2010**, *46*, 3511.

(4) (a) Cornwell, D. J.; Smith, D. K. *Mater. Horiz.* **2015**, *2*, 279. (b) Babu, S. S.; Praveen, V. K.; Ajayaghosh, A. *Chem. Rev.* **2014**, *114*, 1973. (c) Dawn, A.; Shiraki, T.; Haraguchi, S.; Tamaru, S.-I.; Shinkai, S. *Chem. - Asian J.* **2011**, *6*, 266.

(5) (a) van Esch, J. H. *Langmuir* **2009**, *25*, 8392. (b) Dastidar, P. *Chem. Soc. Rev.* **2008**, *37*, 2699. (c) Zurcher, D. M.; McNeil, A. J. *J. Org. Chem.* **2015**, *80*, 2473.

(6) Gupta, J. K.; Adams, D. J.; Berry, N. G. *Chem. Sci.* **2016**, *7*, 4713.

(7) For the United States ban on lead paint, see: Ban of Lead-Containing Paint and Certain Consumer Products Bearing Lead-Containing Paint. *Code of Federal Regulations*, Part 1303, Title 16, 1977.

(8) (a) Lidsky, T. I.; Schneider, J. S. *Brain* **2003**, *126*, 5. (b) Committee on Environmental Health. *Pediatrics* **2005**, *116*, 1036.

(9) Environmental Protection Agency regulations on residential property renovation: (a) Environmental Protection Agency. Small Entity Compliance Guide to Renovate Right: EPA's Lead-Based Paint Renovation, Repair, and Painting Program; Notice of Availability. *Fed Regist.* **2008**, *73*, 21692. (b) EPA. *Fed. Regist.* **2009**, *74*, 34257. (c) Residential Property Renovation. *Code of Federal Regulations*, Part 745, Title 40, Subpart E, 1998. (d) Kessel, I.; O'Connor, J. T. *Getting the Lead Out: The Complete Resource for Preventing and Coping with Lead Poisoning*; Perseus: Cambridge, 2001.

(10) Korfmacher, K. S.; Dixon, S. *Environ. Res.* **2007**, *104*, 241.

(11) (a) Palma, C.-A.; Cecchini, M.; Samorì, P. *Chem. Soc. Rev.* **2012**, *41*, 3713. (b) Mellot-Draznieks, C. J. *J. Mater. Chem.* **2007**, *17*, 4348. (c) Price, S. L.; Price, L. S. In *Solid State Characterization of Pharmaceuticals*; Storey, R. A., Ymén, I., Eds.; Blackwell Publishing Ltd: Oxford, 2011; pp 427−450. (d) Price, S. L. *Adv. Drug Delivery Rev.* **2004**, *56*, 301.

(12) (a) Sun, X.; Sun, Y.; Yu, J. *Cryst. Res. Technol.* **2015**, *50*, 293. (b) Ibiapino, A. L.; Seiceira, R. C.; Pitaluga, A., Jr.; Trindade, A. C.; Ferreira, F. F. *CrystEngComm* **2014**, *16*, 8555. (c) Shim, H. M.; Koo, K.-K. *Cryst. Growth Des.* **2014**, *14*, 1802.

(13) (a) Bravais, A. *Études Cristallographiques*; Gauthier-Villars: Paris, 1866. (b) Friedel, G. *Bull. Soc. Fr. Mineral.* **1907**, *30*, 326. (c) Donnay, J. D. H.; Harker, D. *Am. Mineral.* **1937**, *22*, 446.

(14) (a) Hartman, P.; Bennema, P. *J. Cryst. Growth* **1980**, *49*, 145. (b) Hartman, P. *J. Cryst. Growth* **1980**, *49*, 157. (c) Hartman, P. *Crystal Growth: An Introduction*; North Holland Publishing Co.: Amsterdam, 1973. (d) Hartman, P.; Perdok, W. G. *Acta Crystallogr.* **1955**, *8*, 521. (e) Hartman, P.; Perdok, W. G. *Acta Crystallogr.* **1955**, *8*, 49.

(15) Attachment energy (AE) is defined as the energy released per mole when a new slice with a thickness of d_{hkl} is added to an existing crystal face.

(16) For representative examples, see: (a) Lazo Fraga, A. R.; Ferreira, F. F.; Lombardo, G. M.; Punzo, F. *J. Mol. Struct.* **2013**, *1047*, 1. (b) Kiang, Y.-H.; Yang, C.-Y.; Staples, R. J.; Jona, J. *Int. J. Pharm.* **2009**, *368*, 76. (c) Coombes, D. S.; Catlow, C. R. A.; Gale, J. D.; Rohl, A. L.; Price, S. L. *Cryst. Growth Des.* **2005**, *5*, 879. (d) Brunsteiner, M.; Price, S. L. *Cryst. Growth Des.* **2001**, *1*, 447. (e) Docherty, R.; Clydesdale, G.; Roberts, K. J.; Bennema, P. *J. Phys. D: Appl. Phys.* **1991**, *24*, 89.

(17) (a) Weiss, R. G. *J. Am. Chem. Soc.* **2014**, *136*, 7519. (b) Kumar, D. K.; Steed, J. W. *Chem. Soc. Rev.* **2014**, *43*, 2080.

(18) For example, see: Adams, D. J.; Morris, K.; Chen, L.; Serpell, L. C.; Bacsa, J.; Day, G. M. *Soft Matter* **2010**, *6*, 4144.

(19) Hanabusa, K.; Yamada, M.; Kimura, M.; Shirai, H. *Angew. Chem., Int. Ed. Engl.* **1996**, *35*, 1949.

(20) Cambridge Structural Database, version 5.35; http://www.ccdc.cam.ac.uk/Solutions/CSDSystem/Pages/CSD.aspx.

(21) (a) Adalder, T. K.; Dastidar, P. *Cryst. Growth Des.* **2014**, *14*, 2254. (b) See also refs 3b and 3c.

(22) Diehn, K. K.; Oh, H.; Hashemipour, R.; Weiss, R. G.; Raghavan, S. R. *Soft Matter* **2014**, *10*, 2632.

(23) Muro-Small, M. L.; Chen, J.; McNeil, A. J. *Langmuir* **2011**, *27*, 13248.

(24) Materials Studio, version 6.0; http://accelrys.com/products/materials-studio/index.html.

(25) Constrained geometry optimizations were previously shown to most accurately predict the relative energy differences between polymorphs: Mitchell-Koch, K. R.; Matzger, A. J. *J. Pharm. Sci.* **2008**, *97*, 2121.

(26) (a) Rappe, A. K.; Casewit, C. J.; Colwell, K. S.; Goddard, W. A.; Skiff, W. M. *J. Am. Chem. Soc.* **1992**, *114*, 10024. (b) Casewit, C. J.; Colwell, K. S.; Rappe, A. K. *J. Am. Chem. Soc.* **1992**, *114*, 10035. (c) Casewit, C. J.; Colwell, K. S.; Rappe, A. K. *J. Am. Chem. Soc.* **1992**, *114*, 10046.

(27) Pb(IV) often exhibits square planar coordination geometries, and Pb(II) sandwich compounds show linear coordination geometry.

(28) Large changes between the optimized and experimental structures were observed during an unconstrained geometry optimization (Table S1).

(29) We found that bond lengths did not change after optimization, regardless of the way bonding (localized versus delocalized) is represented (Figure S28 and Table S10).

(30) We found that morphology prediction directly from the constrained geometry optimization was more time-consuming and resulted in only minor changes (Figure S16 and Tables S6 and S7).

(31) (a) Ng, S. W. *Acta Crystallogr., Sect. C: Cryst. Struct. Commun.* **1999**, *55*, IUC9900091. (b) Trindade, T.; O'Brien, P.; Zhang, X.-M.; Motevalli, M. *J. Mater. Chem.* **1997**, *7*, 1011.

(32) Mohammadnezhad, G.; Ghanbarpour, A. R.; Amini, M. M.; Ng, S. W. *Acta Crystallogr., Sect. E: Struct. Rep. Online* **2010**, *66*, m529.

(33) Several examples of lead(II) gelators have since been described: (a) Knerr, P. J.; Branco, M. C.; Nagarkar, R.; Pochan, D. J.; Schneider,

DOI: 10.1021/jacs.6b06269
J. Am. Chem. Soc. 2016, 138, 12228−12233

J. P. *J. Mater. Chem.* **2012**, *22*, 1352. (b) Wei, T.; Dang, J.; Lin, Q.; Yao, H.; Liu, Y.; Zhang, W.; Ming, J.; Zhang, Y. *Sci. China: Chem.* **2012**, *55*, 2554. (c) Yao, H.; You, X.-M.; Lin, Q.; Li, J.-J.; Guo, Y.; Wei, T.-B.; Zhang, Y.-M. *Chin. Chem. Lett.* **2013**, *24*, 703. (d) Sengupta, S.; Mondal, R. *J. Mater. Chem. A* **2014**, *2*, 16373. (e) Knichal, J. V.; Gee, W. J.; Burrows, A. D.; Raithby, P. R.; Wilson, C. C. *CrystEngComm* **2015**, *17*, 8139.

(34) Yu, G.; Yan, X.; Han, C.; Huang, F. *Chem. Soc. Rev.* **2013**, *42*, 6697.

(35) Zhu, L.-H.; Zeng, M.-H.; Ng, S. W. *Acta Crystallogr., Sect. E: Struct. Rep. Online* **2005**, *61*, m1082.

(36) Anne, M. X-ray Diffraction of Poorly Organized Systems and Molecular Gels. In *Molecular Gels: Materials with Self-Assembled Fibrillar Networks*; Weiss, R. G., Terech, P., Eds.; Springer: Dordrecht, The Netherlands, 2006; p 357.

(37) It is more common to find crystal structures that do not match the gel state: (a) Sureshan, K. M.; Vidyasagar, A. *Angew. Chem., Int. Ed.* **2015**, *54*, 12078. (b) Chen, J.; Kampf, J. W.; McNeil, A. J. *Langmuir* **2010**, *26*, 13076. (c) Das, U. K.; Trivedi, D. R.; Adarsh, N. N.; Dastidar, P. *J. Org. Chem.* **2009**, *74*, 7111. (d) Wang, Y.; Tang, L.; Yu, J. *Cryst. Growth Des.* **2008**, *8*, 884. (e) Kumar, D. K.; Jose, D. A.; Das, A.; Dastidar, P. *Chem. Commun.* **2005**, 4059. (f) Sangeetha, N. M.; Bhat, S.; Choudhury, A. R.; Maitra, U.; Terech, P. *J. Phys. Chem. B* **2004**, *108*, 16056. (g) Kumar, D. K.; Jose, D. A.; Dastidar, P.; Das, A. *Langmuir* **2004**, *20*, 10413. (h) Ballabh, A.; Trivedi, D. R.; Dastidar, P. *Chem. Mater.* **2003**, *15*, 2136. (i) van Esch, J.; Schoonbeek, F.; de Loos, M.; Kooijman, H.; Spek, A. L.; Kellogg, R. M.; Feringa, B. L. *Chem. - Eur. J.* **1999**, *5*, 937. (j) Ostuni, E.; Kamaras, P.; Weiss, R. G. *Angew. Chem., Int. Ed. Engl.* **1996**, *35*, 1324.

(38) 17% v/v MeOH was added to dissolve the sodium dithiocarbamate ligand and speed-up in situ complex formation.

(39) Klean-Strip paint thinner made with mineral spirits. Barr Product No. PA12779.

(40) Rust-Oleum Professional, V7579 Gloss Black, High Performance Protective Enamel.

(41) Kanchi, S.; Singh, P.; Bisetty, K. *Arabian J. Chem.* **2014**, *7*, 11.

(42) Environmental Protection Agency, Office of Pollution Prevention and Toxics. *Distribution of Soil Lead in the Nation's Housing Stock*; EPA 747-R96-002; U.S. Government Printing Office: Washington, DC, 1996.

(43) The cgc varies with the quantity of paint in the sample; as a result, a new cgc must be measured for each lead concentration targeted.

(44) The instructions on 3M's LeadCheck caution that positive signals for lead can be obtained for samples with concentrations as low as 600 ppm.

DOI: 10.1021/jacs.6b06269
J. Am. Chem. Soc. 2016, 138, 12228−12233